Acta Biomaterialia 129 (2021) 169–177

Contents lists available at ScienceDirect

Acta Biomaterialia

journal homepage: www.elsevier.com/locate/actbio

Full length article

Multiscale and multimodal X-ray analysis: Quantifying phase orientation and morphology of mineralized turkey leg tendons

Anjani K. Maurya[a,b,c,1], Annapaola Parrilli[a], Tatiana Kochetkova[d], Jakob Schwiedrzik[d], Alex Dommann[a,c], Antonia Neels[a,e,*]

[a] Empa, Swiss Federal Laboratories for Materials Science and Technology, Center for X-Ray Analytics, Lerchenfeldstrasse 5, St. Gallen 9014, Switzerland
[b] Empa, Swiss Federal Laboratories for Materials Science and Technology, Laboratory for Biomimetic Membranes and Textiles, Lerchenfeldstrasse 5, St. Gallen 9014, Switzerland
[c] ARTORG Center for Biomedical Engineering Research, University of Bern, Murtenstrasse 50, Bern 3008, Switzerland
[d] Empa, Swiss Federal Laboratories for Materials Science and Technology, Laboratory for Mechanics of Materials & Nanostructures, Feuerwerkerstrasse 39, Thun 3603, Switzerland
[e] Department of Chemistry, University of Fribourg, Avenue de l'Europe 20, Fribourg 1700, Switzerland

ARTICLE INFO

Article history:
Received 30 January 2021
Revised 16 May 2021
Accepted 19 May 2021
Available online 27 May 2021

Keywords:
Hierarchical structure
Bone and tendons
Degree of orientation
Micro-CT
SAXS and WAXD

ABSTRACT

Fibrous biocomposites like bone and tendons exhibit a hierarchical arrangement of their components ranging from the macroscale down to the molecular level. The multiscale complex morphology, together with the correlated orientation of their constituents, contributes significantly to the outstanding mechanical properties of these biomaterials. In this study, a systematic road map is provided to quantify the hierarchical structure of a mineralized turkey leg tendon (MTLT) in a holistic multiscale evaluation by combining micro-Computed Tomography (micro-CT), small-angle X-ray scattering (SAXS), and wide-angle X-ray diffraction (WAXD). We quantify the interplay of the main MTLT components with respect to highly ordered organic parts such as fibrous collagen integrating inorganic components like hydroxyapatite (HA). The microscale fibrous morphology revealing different types of porous features and their orientation was quantified based on micro-CT investigations. The quantitative analysis of the alignment of collagen fibrils and HA crystallites was established from the streak-like signal in SAXS using the Ruland approach and the broadening of azimuthal profiles of the small and wide-angle diffraction peaks. It has been in general agreement that HA crystallites are co-aligned with the nanostructure of mineralized tissue. However, we observe relatively lower degree of orientation of HA crystallites compared to the collagen fibrils, which supports the recent findings of the structural interrelations within mineralized tissues. The generic multiscale characterization approach of this study is relevant to any hierarchically structured biomaterials or bioinspired materials from the μm-nm-Å scale. Hence, it gives the basis for future structure-property relationship investigations and simulations for a wide range of hierarchically structured materials.

Statement of significance

Many fibrous biocomposites such as tendon, bone, and wood possess multiscale hierarchical structures, responsible for their exceptional mechanical properties. In this study, the 3-dimensional hierarchical structure, the degree of orientation and composition of mineralized tendon extracted from a turkey leg were quantified using a multimodal X-ray based approach combining small-angle X-ray scattering and wide-angle X-ray diffraction with micro-Computed Tomography. We demonstrate that hydroxyapatite (HA) domains are co-aligned with the nanostructure of mineralized tissue. However, the lower degree of orientation of HA crystallites was observed when compared to the collagen fibrils. The generic multiscale characterization approach of this study is relevant to any hierarchically structured biomaterials or bioinspired materials from the micrometer over the nanometer to the Angström scale level.

https://doi.org/10.1016/j.actbio.2021.05.022
1742-7061/

1. Introduction

Many biological composite materials such as wood, bone, and tendons possess a hierarchical structure spanning multiple scales. The excellent mechanical properties of such materials are attributed to their hierarchical structure ranging from micrometer down to the molecular level, the respective fiber orientation, and tissue composition [1,2]. In particular, tendons are dense fibrous connective tissues between muscle fibers and bones [1,3]. In the body, tendons are constantly subjected to dynamic mechanical loads while they transmit the mechanical force of the muscle to the bones. Hence, tendons demonstrate viscoelasticity and high mechanical strength, especially in tension [4]. The nanostructure of the tendon is composed of unidirectionally aligned collagen fibrils, made of cross-linked collagen molecules packed in a staggered fashion [5]. In the case of calcification, mineral crystals nucleate preferably in the gap zones between the collagen fibrils [6,7]. Furthermore, groups of such mineralized collagen fibrils form the collagen fiber, fiber bundles form the fascicle, and finally, a group of fascicles form the tendon [8]. The tendon cells, the tenocytes, form a complex network that envelops collagen fibers and penetrates between the fibrils [9].

The overall hierarchical structure of the tendon along with the orientation of the collagen fibrils is extremely important for its mechanical properties. The mechanical properties of tendons are highly compromised due to rupture or other tendon diseases, which result in patients' pain and reduced mobility and functionality [10]. Injury and degeneration may change the dimensions of the tendon tissue due to the change in the internal structure [11,12]. Therefore, the hierarchical structure and the orientation of the collagen fibrils of the tendon tissue are not only important for understanding its mechanical behavior but also for determining the pathophysiology of the tendon tissue.

In the past, various methods have been used for the structural characterization of tendon tissue. Computed tomography (CT) [13] and magnetic resonance imaging (MRI) [14,15] are the most commonly used techniques providing information about the tendon circumferential and interstitial morphological zones. These techniques provide 3D structural information on a microscale. Electron microscopy techniques [16,17] are used to get the information in nanoscale. However, these techniques are destructive and only provide very local information. Polarised Raman spectroscopy [18–21] and polarised Fourier-transform infrared spectroscopy [22,23] provide insights on fibril orientation and composition but it is challenging to obtain quantitative measures of composition and microstructure.

Small-angle X-ray scattering (SAXS) and wide-angle X-ray diffraction (WAXD) are the techniques providing structural information in the nano- to Ångström-scale range inside the tendon tissue [6,7,24,25]. Fratzl et al. have utilized SAXS to study the structure of wet, dry, and mineralized turkey leg tendons (MTLT) [6]. They studied the mineralization process and concluded that the mineral is first nucleated in the gap zones but continues to extend into the packed collagen fibril zone at very high degrees of mineralization [6,26]. Gupta et al. have studied the mineralized microstructure of calcified avian tendons by SAXS to determine the size, shape, and orientation of the mineral crystals [25]. White et al. have investigated the collagen-mineral axial relationship in calcified turkey leg tendons by X-ray and neutron diffraction methods and reported that the minerals are arranged with the same axial periodicity as the collagen and occupy the gap region of the collagen structure [7]. Although the individual levels in the hierarchical tendon structure and the related mineralization processes have already been investigated in the past, the degree of orientation at the various length scales is only qualitatively discussed. The detailed quantification of orientation at different length scales is particularly important to understand the mechanical response of the tendon tissue under applied forces in healthy or injured tendons [18,24,27].

In this study, we have investigated the micro-nano-Ångström scale structure of a mineralized tendon tissue extracted from a turkey leg. The combination of non-destructive X-ray based methods such as micro-CT, SAXS, and WAXD provide structural (phase) information along with the corresponding phase orientations at multiple length scales. We have concentrated on the data analysis to quantify the orientation of the collagen fibers, fibrils and hydroxyapatite (HA) crystallites. The mineralized tendon is an ideal model system as its structure and related properties are similar to other systems such as bones [6,17,25,27,28]. Therefore, this study is also relevant as a generic multiscale characterization methodology for any of such hierarchical structures.

2. Materials and methods

2.1. Sample preparation

The mineralized tendons were extracted from the turkey leg obtained from a local abattoir. The tendons were cleaned from the soft tissue and cut with a diamond band saw under constant water irrigation (Exakt, Norderstedt, Reichert-Jung, Germany). The tendon piece of ~1.5 mm diameter and 4 mm length was used for micro-CT, SAXS, and WAXD measurements.

2.2. Micro-Computed Tomography (micro-CT)

MTLT sample was investigated by micro Computed Tomography (micro-CT) using an EasyTom XL Ultra 230–160 micro/nano-CT system (RX Solutions, Chavanod France). The scanner operated at 90 kV, 100 μA, rotation step 0.25°, rotation 360°, and spatial resolution of 400 nm/pixel.

2.3. Small-angle X-ray scattering (SAXS)

SAXS measurements were performed with a Bruker Nanostar system (Bruker AXS GmbH, Karlsruhe, Germany) equipped with a micro-focused X-ray Cu source (wavelength of CuKα with 1.5406 Å) and a VÅNTEC-2000 detector. The X-ray beam is pinholes collimated (beam diameter of about 0.5 mm) with a custom-made semitransparent beamstop. The VÅNTEC-2000 is a gaseous avalanche-based detector with arrays of 2048 × 2048 pixels with a pixel size of 68 × 68 μm^2. The instrument operates in moderate vacuum conditions of about 10^{-2} mbar pressure to reduce the air scattering and providing a resolvable q-range of 0.07–8.00 nm^{-1} by combining sample-to-detector distances (SDD) of 107 cm and 27 cm. The scattering experiment performed at the SDD of 27 cm could be called medium-angle X-ray scattering (MAXS) which bridges the gap between the SAXS and WAXD. For simplicity, we refer to this measurement also as SAXS in this study. The sample was measured for 3600 s for both SDDs. 1D profiles were extracted using the Bruker software DIFFRAC.EVA (Bruker AXS, version 4.1). The background was subtracted after normalising the 1D radial profiles to the transmitted intensity.

* Corresponding author at: Empa, Swiss Federal Laboratories for Materials Science and Technology, Center for X-Ray Analytics, Lerchenfeldstrasse 5, St. Gallen 9014, Switzerland.

E-mail address: antonia.neels@empa.ch (A. Neels).

[1] Present address: Stanford Synchrotron Radiation Lightsource, SLAC National Accelerator Laboratory, Menlo Park, CA, 94025, USA.

2.4. Wide-angle X-ray diffraction (WAXD)

Wide-angle X-ray diffraction (WAXD; STOE IPDS-II, MoKα radiation with λ = 0.71073 Å, a source at 40 mA, 50 kV, exposures for 30 min in a beam with a diameter of 0.5 mm in transmission mode) was used to study the crystal structure and degree of mineral crystals alignment with respect to the collagen fiber orientation. The sample was fixed on the goniometer head and then aligned perpendicular to the X-ray beam. The WAXD profile was recorded on an Image Plate Detector System (IPDS) with a 340 mm diameter and placed at a distance of 200 mm from the sample. 2D diffraction images have been recorded covering a 2θ range from 3 to 40°. 1D radial profiles in equatorial and meridional direction and the azimuthal profile for the hydroxyapatite (002) reflection were extracted. The Crystallography Open Database (COD) is used for indexing.

2.5. Orientation analysis of different phases

The orientation analysis of structural phases present in the tendon tissues at various length scales was carried out using micro-CT, SAXS, and WAXD methods. SAXS and WAXD are performed on the same sample as the micro-CT. While by micro-CT a 3D representative volume of interest (VOI) of 0.2 × 0.2 × 0.2 mm^3 was investigated for the statistical analysis, transmission WAXD and SAXS randomize over a slightly larger volume fraction based on a 0.5 mm X-ray beam diameter and the sample thickness (~1.5 mm). The details of the correlative positional information are given in the supporting section S2. As micro-CT focuses on a smaller but representative VOI, the correlative assessment of the multiscale relative orientation and positioning is guaranteed.

2.5.1. Microscale orientation of collagen fibers by micro-CT

A VOI of 500 × 500 × 500 pixels (0.2 × 0.2 × 0.2 mm^3) was selected in the inner portion of the sample, being representative for the total investigated sample volume (0.5 × 0.5 × 0.3 mm^3), and used for the orientation analysis. The preferred orientation of the elongated lacunae was calculated in ImageJ [29] using the image stacks in the xz and yz plane of the VOI. The Directionality plugin with a local gradient orientation was used and the results demonstrated the preferred vertical orientation of the collagen fibers.

2.5.2. Nanoscale orientation of collagen fibrils and HA domains by SAXS

SAXS provides the nanostructure information on a length scale of about 1–100 nm. Therefore, it is ideal to decode the average orientation of the collagen fibrils coupled with the periodically arranged elongated HA domains and the HA domains separately. In this study, HA domains refer to the global size and shape of HA crystallites, which provide an electronic contrast at the nanoscale.

(1) *Determination of misorientation width (MOW) by the Ruland method*
The Ruland method analyses the streak-like signal observed in the orthogonal direction of the tendon fiber alignments and determines the misorientation width (MOW) of the fibril coupled with elongated HA domains in the collagen fiber. The details of the Ruland method are described elsewhere [30].

(2) *Quantification of the degree of orientation using the azimuthal broadening of the peak*

The degree of orientation is determined by extracting the full width at half maximum (FWHM) of the azimuthal profile by Gaussian fitting of the small-angle or wide-angle diffraction peaks. The degree of orientation (π) is determined by using Eq. (1) [31].

$$\pi = \frac{(180 - FWHM)}{180} \quad (1)$$

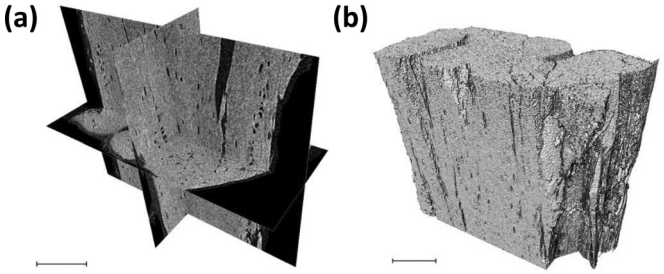

Fig. 1. Micro-CT analysis of the MTLT sample. (a) Orthogonal view of the cross-sections; (b) 3D model of the acquired volume of the sample. Scale bars = 0.1 mm.

π =1 for perfectly aligned and 0 for non-aligned samples.

2.5.3. Ångström-scale orientation of HA crystallites by WAXD

From the X-ray diffraction data obtained by a 2D diffraction experiment covering a d-spacing range between 30.0 and 1.0 Å, structural information is gained for present crystallographic phases and their preferred orientation with respect to each other and the tendon alignment. The HA crystallite orientation is derived using Eq. (1) on azimuthal scans on the HA (002) reflection using the 2D X-ray diffraction data [16]. The presence of 2 phases, whose periodicity is close to perpendicular, permits to derive their exact alignment with respect to each other.

2.6. Statistical analysis

Statistical analysis was performed using R [32]. Nonparametric statistical tests were used due to the limited sample number. Significant differences between datasets were tested using the Wilcoxon rank sum test. Measurements are reported as mean ± standard deviation.

3. Results and discussion

The MTLT sample was investigated for µm-nm-Å scale levels of the hierarchical structure along with the different phase information and orientation which critically influence its mechanical properties. The detailed quantification was performed by state-of-the-art lab-based micro-CT, SAXS, and WAXD experiments.

3.1. Microscale morphology and orientation by micro-CT

At the micrometric level, two zones of tissue with different structures can be distinguished in MTLT: the circumferential (CIR) and interstitial (INT) zones [13]. The collagen fibers are smaller in diameter and densely packed in the CIR zone, while they are larger and less packed in the INT zone [9]. Tenocytes are arranged longitudinally along the fibers in more elongated lacunae in the CIR zones and more cuboidal lacunae in the INT zones.

Micro-scale information of MTLT was obtained with micro-CT. Micro-CT analysis allowed obtaining a stack of cross-section images of 16-bit that represent the volume of the sample as shown in Fig. 1.

The two morphological zones CIR and INT of the mineralized tendon tissues are usually classified according to the different diameters of the fibers (smaller in diameter and denser in the circumferential zone and larger and less packed in the interstitial zone). In our study, the identification of these two areas is possible due to the presence of a different type of cellular lacunae. The lacunae of the tenocytes in the CIR zone have a shape similar to that of the osteocytes in the bone, while the cells in the INT zone are cubic in shape and positioned along with columns as can be seen in Fig. 2.

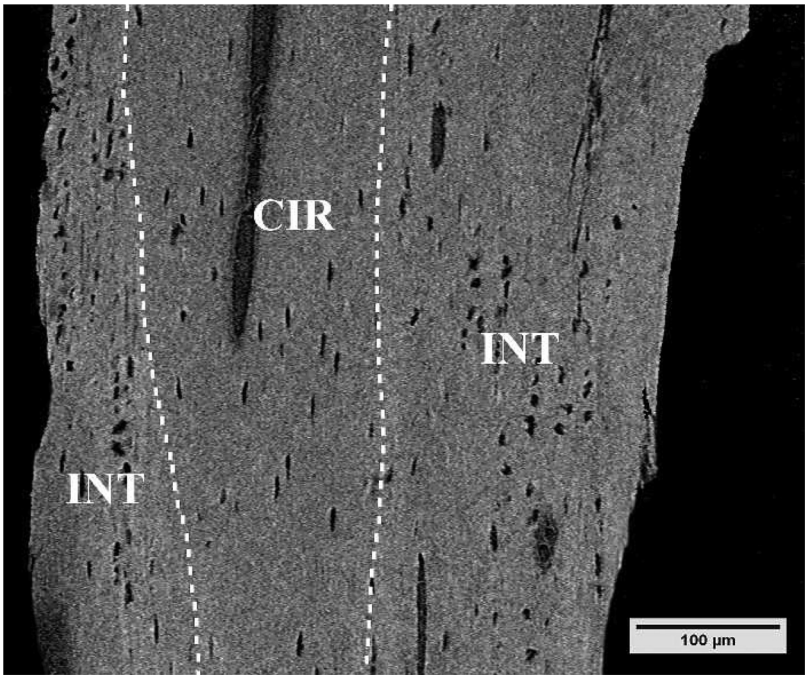

Fig. 2. Coronal micro-CT section (xz axes) of the sample. Circular to elongate resorption cavities are present started from enlarged tenocytes associated with the onset of mineralization in the circumferential zone (CIR), while cubic-shaped lacunae are present in the interstitial zone (INT). Scale bar = 100 µm.

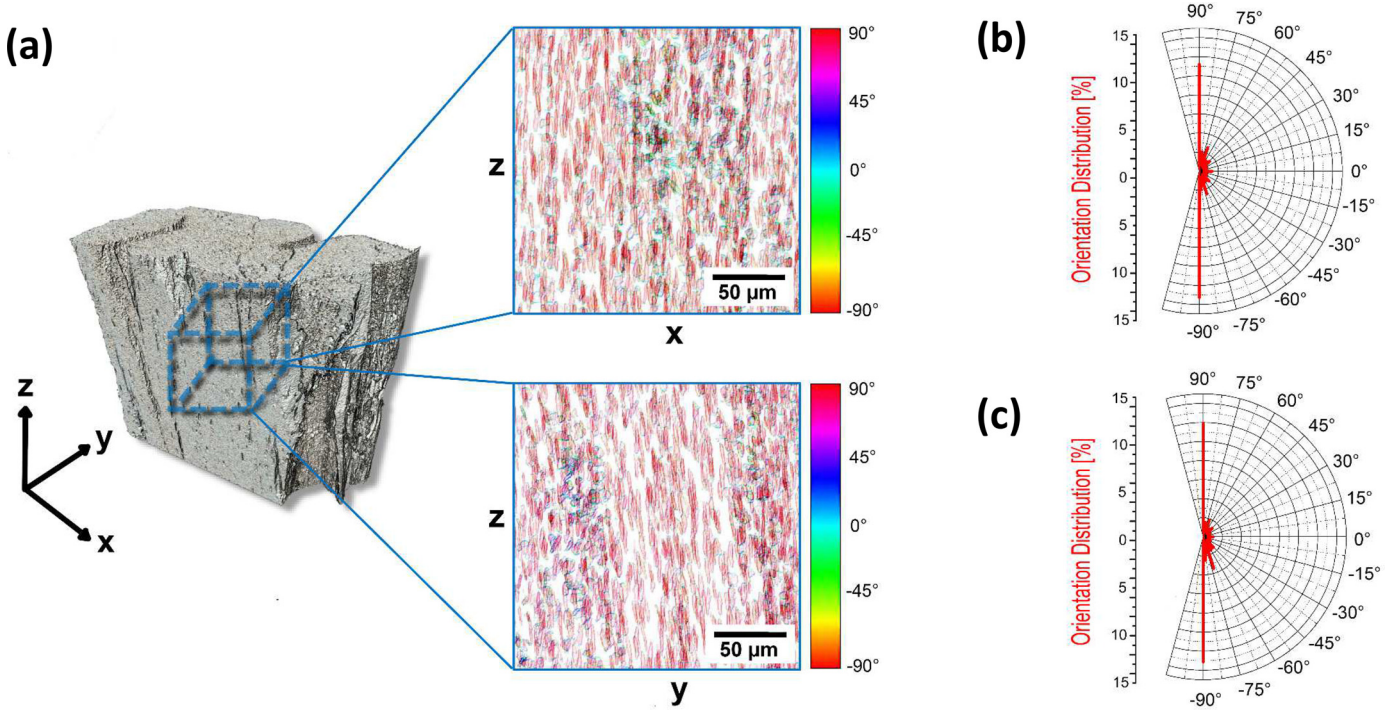

Fig. 3. Orientation analysis of the fibers. (a) The volume of interest (VOI) of 500 × 500 × 500 pixels was cut in the xz and yz planes; the overlapped images of the entire datasets in the two planes after the application of the directionality plugin of ImageJ are shown in the onsets colored as the color-coded orientation angles. (b) The graph of the orientation distribution of the VOI stacks in the xz plane. The percentage of frequency is determined by the high of the red line for each angle according to the value of the graduated axis (c) The graph of the orientation distribution of the VOI stacks in the yz plane. (For interpretation of the references to color in this figure legend, the reader is referred to the web version of this article.)

In addition, as the cells of the mineralized tendon are positioned along the collagen fibers and along with the fiber bundles, the elongated shape of their lacunae was used to make an indirect calculation of the collagen fiber orientation.

The orientation was calculated in the two orthogonal planes along the z-axis (Fig. 3). The distribution of the orientation indicates the number of lacunae in a given direction. In the case of preferred orientation, the graph shows a peak in that orientation. In both considered planes, the peak of the orientation is detected at 90° or −90° demonstrating the preferred vertical alignment of fibers.

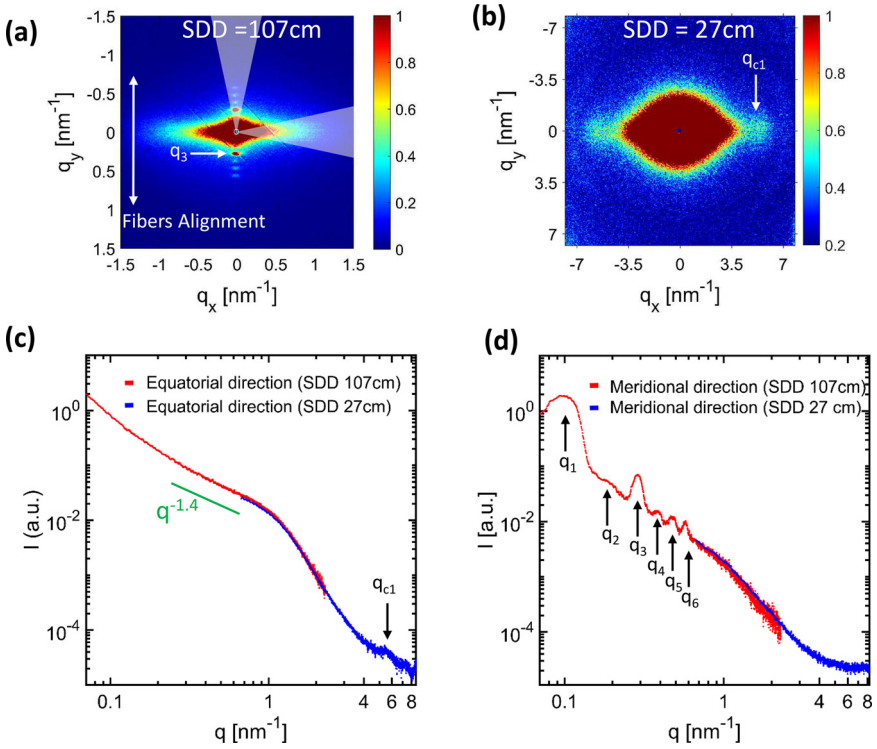

Fig. 4. 2D-SAXS profiles measured at SDDs of (a) 107 cm and (b) 27 cm. 1D-radial profiles stitched together for SDDs of 107 cm and 27 cm in (c) equatorial direction (normal to fiber alignment) and (d) meridional direction (along the fiber alignment). q_1-q_6 indicates the first to sixth order peaks due to the periodicity of HA domains along the fiber alignment. q_{c1} is the first order peak due to collagen fibrils periodicity orthogonal to fiber alignment.

3.2. Nanoscale structure and orientation quantification by SAXS

Nanostructural information is obtained by SAXS. 2D-SAXS profiles of the MTLT were measured at two different SDDs to gain the information in the q-range of 0.07–8.0 nm^{-1}. The 2D-SAXS profiles for SDDs of 107 cm and 27 cm are shown in Fig. 4(a) and (b), respectively. The profile measured at the SDDs of 107 cm shows the streak-like signal (diffuse scattering) in the equatorial direction while peaks occur in the meridional direction. The streak-like signal is originated due to the alignment of collagen fibrils and the plate-like elongated hydroxyapatite (HA) domains along with the collagen fiber inside the tendon tissue in the nanoscale (see Fig. 5) [6]. The peaks in the meridional direction relate to the periodicity of the HA domains along the fibril collagen alignment direction [33,34]. The HA crystallites form in the gap regions (HA domains) between the triple-collagen helixes [6,7].

The 2D-SAXS profile measured at the SDD of 27 cm shows the streak-like signal in the equatorial direction along with the peak being indicated by q_{c1} in Fig. 4(b). This observed peak is related to lateral packing of the collagen fibrils. No peaks in equatorial direction were observed in small-angle due to the lower resolution related to the small SDD of 27 cm.

Nanostructural information was further quantified by extracting the 1D-radial profile (30° wedge azimuthal integration) in equatorial and meridional directions. The 1D-radial profiles stiched for SDDs of 107 cm and 27 cm in equatorial and meridional directions are shown in Fig. 4(c) and (d), respectively. In the equatorial direction, exponential decay is observed with a Porod exponent of −1.4 in the q-range of 0.4–0.6 nm^{-1} (see Fig. 4(c)). The solid cylinder object scatters with a Porod exponent of −1 [35]. The deviation is most probably due to the contribution of HA crystals and the flexible structure of collagen fibrils [35]. Furthermore, a weak peak is observed at 5.6 nm^{-1} (indicated by q_{c1} in Fig. 4(c)) which provides the inter collagen fibril spacing of 12 Å. In the meridional direction, the d-spacing of the periodicity of the HA crystals of 66.1 nm was determined by the 3rd order peak position. A schematic of the nanostructure based on the above finding is shown in Fig. 5(b).

Along with the nanostructure, the orientation at different length scales, influences the overall mechanical properties of the tendon tissue [18,24], was quantified by the following two different methods based on the SAXS data.

3.2.1. Orientation analysis by Ruland streak method

The Ruland streak method is based on the analysis of the streak-like signal in the 2D-SAXS profile [36,37], which originates from the collagen fibrils but is also influenced by the diffuse scattering due to the platelet-like HA domains in small-angle. Therefore, this method provides the misorientation width of the collagen fibrils coupled with HA domain orientation.

To determine the misorientation width, the azimuthal profiles were extracted in the q-range of 0.28 to 1.1 nm^{-1} with a step size of 0.036 nm^{-1} for a 120° azimuthal angle. The exact q-positions where obtained from the azimuthal profiles shown in Fig. 6(a). All extracted azimuthal profiles are shown in Fig. 6(b) together with the Lorentzian fitting of each profile. The azimuthal broadening was determined by the FWHM of the Lorentzian fitting which is plotted in Fig. 6(c) over the inverse of q. The linear fitting provides the misorientation width of (14.0 ± 0.3)° of the collagen fibrils coupled with HA domains.

3.2.2. Degree of orientation quantification from the azimuthal profile of 3rd order peak

The peaks in the meridional direction in the SAXS profile originate from the periodic arrangement of the HA domains in the fiber direction as shown in schematic Fig. 5(b). Therefore, the degree of orientation of these HA domains can be determined using Eq. (1).

To determine the degree of orientation of the HA domains, an azimuthal integration of the 3rd order peak was obtained using

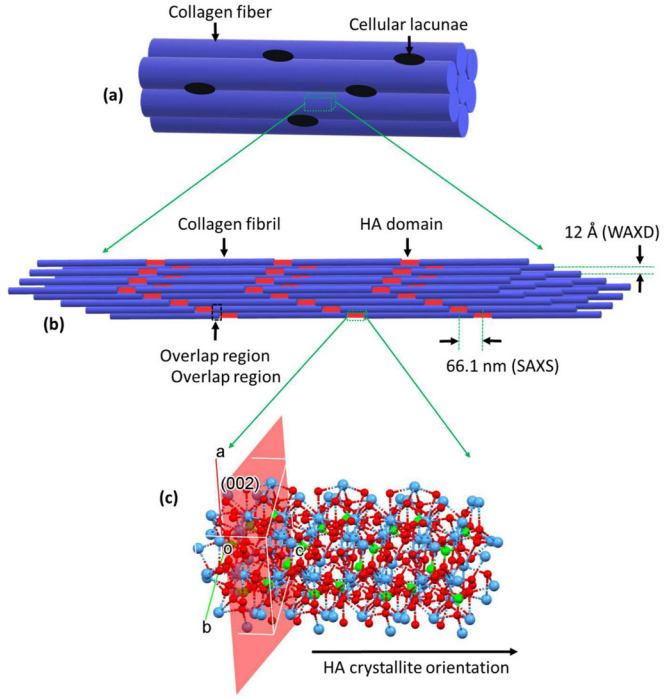

Fig. 5. Schematic of the μm-nm-Å scale structure of a MTLT sample. (a) Microscale morphological structure with collagen fibers and cellular lacunae; (b) Nanoscale structure with collagen fibrils with HA domains; (c) HA crystal structure (atom colors: light blue for Ca, green for P, and red for O). (For interpretation of the references to color in this figure legend, the reader is referred to the web version of this article.)

the q-range of 0.25–0.34 nm^{-1}. Thereafter, the extracted azimuthal profile was fitted with a Gaussian function and the FWHM of the peak was determined. The q-range of the azimuthal profile and the corresponding extracted azimuthal profile together with the Gaussian fitting are shown in Fig. 7(a) and (b), respectively. The degree of orientation was obtained with $\pi = 0.93$, which means that the HA domains are highly aligned along the fiber direction ($\pi = 1$ for 100% alignment and 0 for random orientation).

3.3. Crystallographic phase and orientation analysis by WAXD

The 2D-WAXD pattern for the MTLT sample is shown in Fig. 8(a). The 1D radial profile was extracted in the meridional direction and equatorial direction (30° wedge azimuthal integration indicated in Fig. 8(b)) are plotted in Fig. 8(c). The indexing of the obtained diffraction patterns revealed two phases: crystalline hydroxyapatite (HA) by phase matching with the COD (Crystallography Open Database, hexagonal, $P6_3/m$ with a = 9.424 and c = 6.879 Å) and lateral packing of collagen fibrils with respect to the fiber alignment direction. The lateral inter-fibrillar spacing of 12 Å was derived from the collagen low-angle peak in the equatorial direction, which is the same as the q_{c1} peak observed in the SAXS measurement performed at 27 cm SDD.

The HA crystallites are oriented along the crystallographic c-axis and along the collagen fibril axis as shown in Fig. 5(b) and (c). Therefore, the HA crystal orientation was determined by the azimuthal broadening of the (002) reflection (FWHM = 41.6 ± 0.1°) from the 2D-WAXD profile. The degree of orientation (π) according to Eq. (1) has been calculated with 0.77 for the HA crystallites indicating a lower orientation compared to the nanoscale structures.

3.4. Comparison of the orientation of the different phases at μm-nm-Å scale

In order to compare the orientation of the collagen fiber at the microscopic level, the FWHM of collagen fiber orientation was determined by Lorentzian fitting of the transformed orientation plot (Fig. 3(b) and (c)) in such a way that 0° orientation angle represents the ideal collagen fiber orientation. The transformed plot and the corresponding fitting for xz and yz planes are shown in Fig. S1(a) and (b). The average FWHM of 7.4 ± 1.7° was obtained due to the misorientation of the collagen fibers in xz and yz plane. Furthermore, SAXS and WAXD experiments were repeated at 5 different positions of the same sample to perform the significance test on the different methods. The exact positions of the SAXS and WAXD measurements on the tendon tissue and the corresponding orientation analysis of the corresponding constituent present at the nm-Å scale are described in the supporting section S2. The average outcome of the orientation analysis of the different phases present at μm-nm-Å levels is summarized in Table 1. The indirect collagen fiber misorientation determined by micro-CT provided a very narrow broadening of 7.4 ± 1.7°. The average misorientation width (B_ϕ = 17.0 ± 1.2°) due to the collagen fibrils combined with HA domains obtained from the Ruland method is in the same order

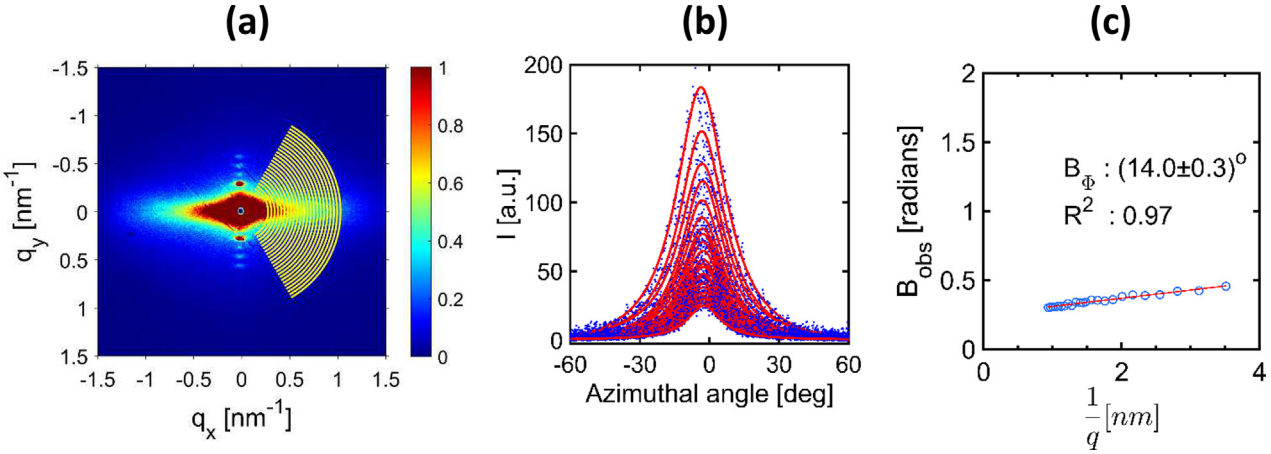

Fig. 6. Determination of the misorientation width of the collagen fibril. (a) 2D-SAXS profile indicating the positions of azimuthal profiles (yellow line) extracted at different q on the streak-like signal; (b) their corresponding azimuthal scans (blue data points) and Lorentzian fits (continuous red line); (c) B_{obs} vs 1/q fitting to determine the misorientation width. (For interpretation of the references to color in this figure legend, the reader is referred to the web version of this article.)

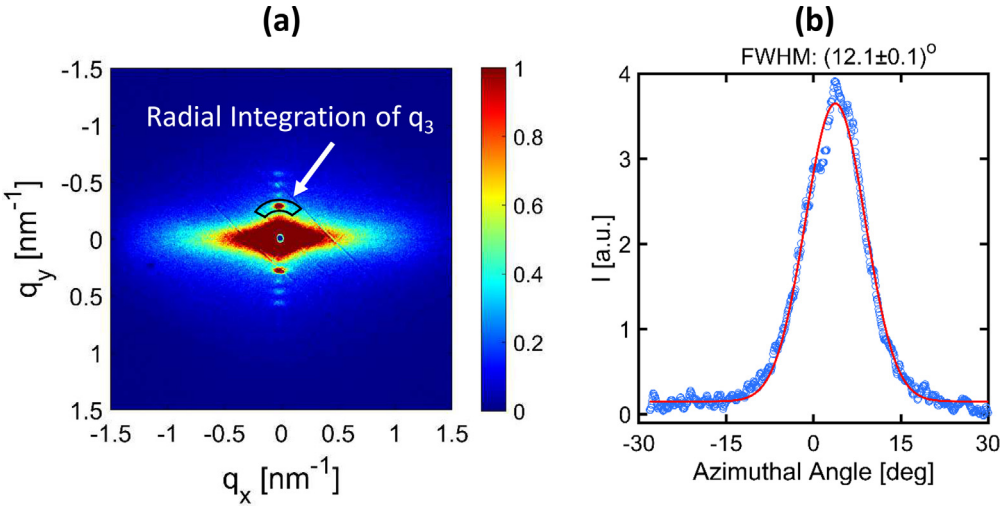

Fig. 7. (a) q and azimuthal range of the radial integration on the 3rd order peak in order to extract the azimuthal profile; (b) corresponding extracted azimuthal profile fitted with a Gaussian function.

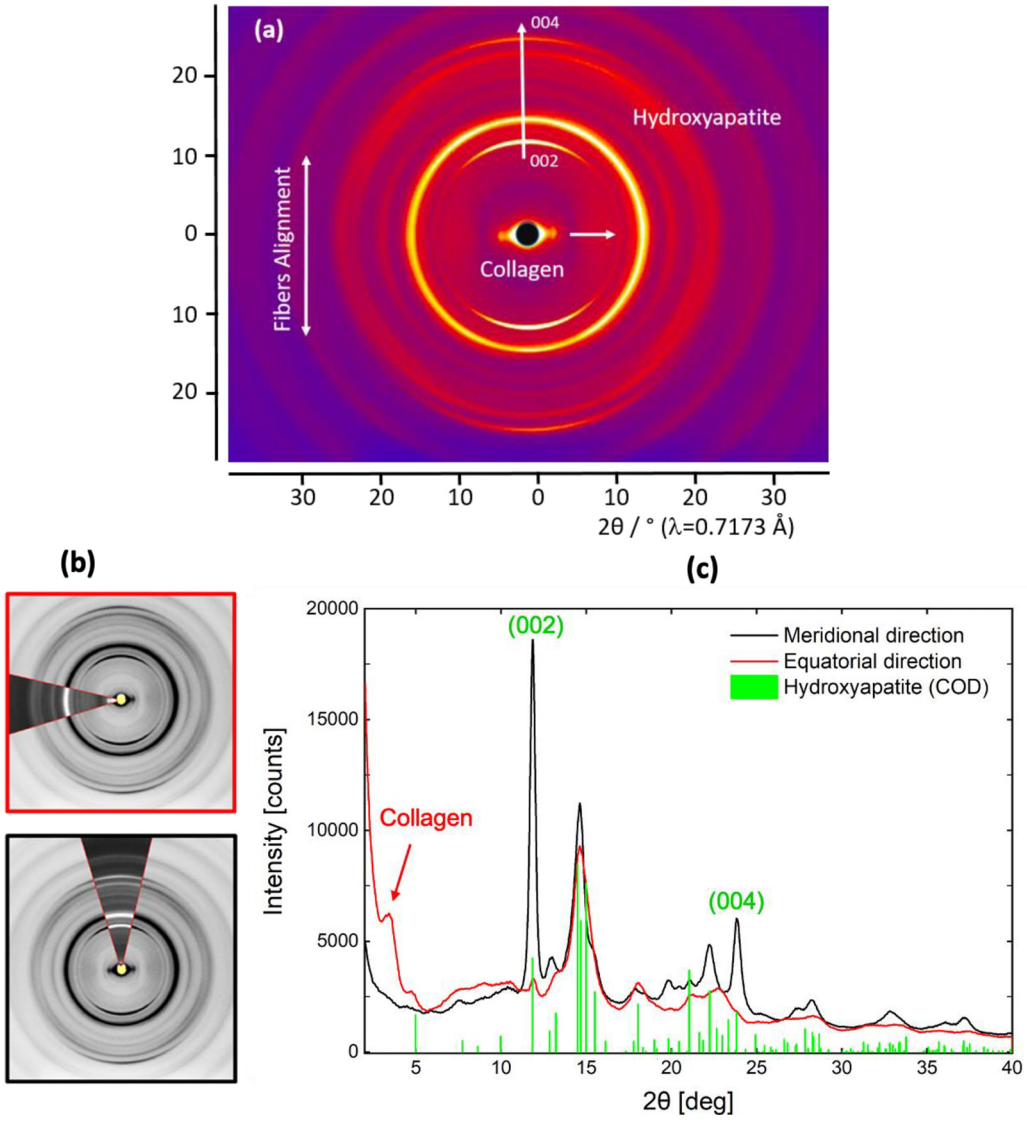

Fig. 8. (a) 2D-WAXD profile showing the ordering features of the collagen fibrils and the HA crystallites with respect to the tendon collagen fiber alignment direction; (b) meridional and equatorial 30° wedge azimuthal integration; (c) 1D diffraction profile in equatorial (red) and meridional (black) direction with respect to the tendon fiber alignment. 2θ corresponds to MoKα radiation with $\lambda = 0.71073$ Å. (For interpretation of the references to color in this figure legend, the reader is referred to the web version of this article.)

Table 1
Comparison of the X-ray multimodalities used for multiscale structural orientation determination.

Method	Oriented structural unit	Scale	Orientation analysis
Micro-CT	Tenocyte lacunae (indirectly collagen fibers orientation)	µm-mm	FWHM = 7.4 ± 1.7o
SAXS	a) Collagen fibril and HA domain (streak-like diffuse scattering in the equatorial direction, Ruland method) b) HA domains in collagen gap zones (Bragg reflection in the meridional direction)	nm	a) Average $B_\phi = 17.0 \pm 1.2°$ b) Average FWHM = 15.4 ± 1.1° ($\pi = 0.92$)
WAXD	HA crystallographic orientation ((002) reflection)	Å	Average FWHM = 41.9 ± 0.7° ($\pi = 0.77$)

of the azimuthal broadening (FWHM = 15.4 ± 1.1°) of the third-order peak due to the periodicity of the HA domains. No significant difference was found between the misorientation widths determined from Ruland and the FWHM of 3rd order peak calculated from SAXS data ($p = 0.05$, Wilcoxon). It means that the orientation of the collagen fibers, fibrils, and the overall orientation related to the periodical HA domains are co-axial along the fiber alignment direction of the tendon tissue.

A significant difference in the degree of orientation of HA domains (π=0.92) and the c-axis of HA crystallites (π=0.77) was observed. It means the c-axis of the HA crystallites is more misoriented compared to the collagen fibrils with respect to the fiber alignment inside the tendon. However, in previous studies, there is a general agreement that the orientation of the crystallographic c-axis of the HA crystallites follows the collagen fibrils in mineralized tissues [7,25]. Nevertheless, a recent publication on the 3D mapping of the orientation of HA crystallites and nanostructures in the human bone has reported the difference in the orientation distribution between the HA crystallites and collagen fibrils [38].

Various scenarios can explain this difference in the degree of orientation of these phases. First, it could be due to the difference in the orientation of the HA crystallites in the interfibrillar locations (outside and along the surfaces of the fibrils) compared to intrafibrillar locations. Such intra- and interfibrillar mineral deposits have recently been observed by Zao et al. by the 3D structural analysis of a mineralized avian leg tendon by Focused Ion Beam Scanning Electron Microscopy (FIB-SEM) [9]. Secondly, an irregularly shaped platelet-like structure of the HA crystals which extends out of the gap zone is observed by some researchers in the case of MTLT [6,39]. The extended crystallites may have more misorientation which reduces the degree of orientation of the HA crystallites.

4. Conclusion

In this study, our emphasis was placed on the quantification of structural and morphological domains and orientations of constituent phases in the hierarchically organized system of MTLT from µm-nm-Å scale by combining micro-CT, SAXS, and WAXD. Using micro-CT, we analyzed the microscale morphology of the mineralized tissue and indirectly quantified the orientation of the collagen fibers. The spacing of 66.1 nm was determined between the adjacent HA domains along the collagen fiber alignment direction from SAXS. The alignment of the collagen fibrils coupled with elongated HA domains and the HA domains separately with respect to fiber alignment direction was quantified by the Ruland method and the azimuthal broadening of the 3rd order SAXS peak, respectively. Furthermore, the hexagonal phase of the HA crystallites (space group $P6_3/m$, $a = 9.424$ and $c = 6.879$ Å) and the lateral spacing of 12 Å for collagen fibrils were determined by WAXD. The degree of orientation of the HA crystallites was quantified by evaluating the azimuthal scan of the (002) reflection. We observed a relatively low degree of orientation along the crystallographic c-axis of the HA crystallites ($\pi = 0.77$) compared to the nanostructure (HA domains, π =0.93) which was previously assumed to be co-axial.

The current study shows a generic approach in detail to quantify the structure, morphology and the degree of orientation of different constituent phases present at the µm-nm-Å level supporting the indication of novel features in a hierarchically structured material. This forms the basis for a detailed understanding of the structure-property relationship and a quality assessment for hierarchically structured biomaterials or bioinspired materials by providing input for finite element simulations.

Declaration of Competing Interest

The authors declare no competing financial interests.

Acknowledgment

The authors are grateful to the Swiss National Foundation project number 173012 (AKM, AN) and Special Focus Area Personalized Health and Related Technologies (SFA PHRT) iDoc Project 2017–304 (TK) for financial support. The authors thank Alexander Groetsch for the primary sample preparation steps.

Supplementary materials

Supplementary material associated with this article can be found, in the online version, at doi:10.1016/j.actbio.2021.05.022.

References

[1] J. Kastelic, A. Galeski, E. Baer, The multicomposite structure of tendon, Connect. Tissue Res. 6 (1) (1978) 11–23.
[2] P. Fratzl, R. Weinkamer, Nature's hierarchical materials, Prog. Mater. Sci. 52 (8) (2007) 1263–1334.
[3] A. Hayes, K. Easton, P. Devanaboyina, J.P. Wu, T. Kirk, D. Lloyd, A review of methods to measure tendon dimensions, J. Orthop. Surg. Res. 14 (2019) 12.
[4] J.H.C. Wang, Mechanobiology of tendon, J Biomech. 39 (9) (2006) 1563–1582.
[5] I. Jäger, P. Fratzl, Mineralized collagen fibrils: a mechanical model with a staggered arrangement of mineral particles, Biophys. J. 79 (4) (2000) 1737–1746.
[6] P. Fratzl, N. Fratzlzelman, K. Klaushofer, Collagen packing and mineralization-an X-ray-scattering investigation of turkey leg tendon, Biophys. J. 64 (1) (1993) 260–266.
[7] S.W. White, D.J.S. Hulmes, A. Miller, P.A. Timmins, Collagen-mineral axial relationship in calcified turkey leg tendon by X-ray and neutron-diffraction, Nature 266 (5601) (1977) 421–425.
[8] F.H. Silver, J.W. Freeman, G.P. Seehra, Collagen self-assembly and the development of tendon mechanical properties, J. Biomech. 36 (10) (2003) 1529–1553.
[9] Z. Zou, T. Tang, E. Macías-Sánchez, S. Sviben, W.J. Landis, L. Bertinetti, P. Fratzl, Three-dimensional structural interrelations between cells, extracellular matrix, and mineral in normally mineralizing avian leg tendon, Proc. Natl. Acad. Sci. 117 (25) (2020) 14102–14109.
[10] S. Thomopoulos, W.C. Parks, D.B. Rifkin, K.A. Derwin, Mechanisms of tendon injury and repair, J. Orthop. Res. 33 (6) (2015) 832–839.
[11] S. Arya, K. Kulig, Tendinopathy alters mechanical and material properties of the Achilles tendon, J. Appl. Physiol. 108 (3) (2010) 670–675.

[12] S.J. Obst, L.J. Heales, B.L. Schrader, S.A. Davis, K.A. Dodd, C.J. Holzberger, L.B. Beavis, R.S. Barrett, Are the mechanical or material properties of the achilles and patellar tendons altered in tendinopathy? A systematic review with meta-analysis, Sports Med. 48 (9) (2018) 2179–2198.
[13] E.M. Spiesz, P. Roschger, P.K. Zysset, Influence of mineralization and microporosity on tissue elasticity: experimental and numerical investigation on mineralized turkey leg tendons, Calcif. Tissue Int. 90 (4) (2012) 319–329.
[14] C. Pierre-Jerome, V. Moncayo, M.R. Terk, MRI of the Achilles tendon: a comprehensive review of the anatomy, biomechanics, and imaging of overuse tendinopathies, Acta Radiol. 51 (4) (2010) 438–454.
[15] A. Chang, T.T. Miller, Imaging of tendons, Sports Health 1 (4) (2009) 293–300.
[16] Y. Xu, F. Nudelman, E.D. Eren, M.J.M. Wirix, B. Cantaert, W.H. Nijhuis, D. Hermida-Merino, G. Portale, P.H.H. Bomans, C. Ottmann, H. Friedrich, W. Bras, A. Akiva, J.P.R.O. Orgel, F.C. Meldrum, N. Sommerdijk, Intermolecular channels direct crystal orientation in mineralized collagen, Nat. Commun. 11 (1) (2020) 5068.
[17] S. Lees, K.S. Prostak, V.K. Ingle, K. Kjoller, The loci of mineral in turkey leg tendon as seen by atomic force microscope and electron microscopy, Calcif. Tissue Int. 55 (3) (1994) 180–189.
[18] T. Kochetkova, C. Peruzzi, O. Braun, J. Overbeck, A.K. Maurya, A. Neels, M. Calame, J. Michler, P. Zysset, J. Schwiedrzik, Combining polarized Raman spectroscopy and micropillar compression to study microscale structure-property relationships in mineralized tissues, Acta Biomater. 119 (2021) 390–404.
[19] A. Masic, L. Bertinetti, R. Schuetz, L. Galvis, N. Timofeeva, J.W.C. Dunlop, J. Seto, M.A. Hartmann, P. Fratzl, Observations of multiscale, stress-induced changes of collagen orientation in tendon by polarized raman spectroscopy, Biomacromolecules 12 (11) (2011) 3989–3996.
[20] L. Galvis, J.W.C. Dunlop, G. Duda, P. Fratzl, A. Masic, Polarized raman anisotropic response of collagen in tendon: towards 3D orientation mapping of collagen in tissues, PLoS ONE 8 (5) (2013) e63518.
[21] L. Van Gulick, C. Saby, H. Morjani, A. Beljebbar, Age-related changes in molecular organization of type I collagen in tendon as probed by polarized SHG and Raman microspectroscopy, Sci. Rep. 9 (1) (2019) 7280.
[22] S.J. Gadaleta, W.J. Landis, A.L. Boskey, R. Mendelsohn, Polarized FT-IR microscopy of calcified turkey leg tendon, Connect. Tissue Res. 34 (3) (1996) 203–211.
[23] G. Bakir, B.E. Girouard, R. Wiens, S. Mastel, E. Dillon, M. Kansiz, K.M. Gough, Orientation matters: polarization dependent IR spectroscopy of collagen from intact tendon down to the single fibril level, Molecules 25 (18) (2020).
[24] A. Groetsch, A. Gourrier, J. Schwiedrzik, M. Sztucki, R.J. Beck, J.D. Shephard, J. Michler, P.K. Zysset, U. Wolfram, Compressive behaviour of uniaxially aligned individual mineralised collagen fibres at the micro- and nanoscale, Acta Biomater. 89 (2019) 313–329.
[25] H.S. Gupta, P. Roschger, I. Zizak, N. Fratzl-Zelman, A. Nader, K. Klaushofer, P. Fratzl, Mineralized microstructure of calcified avian tendons: a scanning small angle X-ray scattering study, Calcif. Tissue Int. 72 (5) (2003) 567–576.
[26] P. Fratzl, M. Groschner, G. Vogl, H. Plenk, J. Eschberger, N. Fratzlzelman, K. Koller, K. Klaushofer, Mineral crystals in calcified tissues - a comparative-study by SAXS, J. Bone Miner. Res. 7 (3) (1992) 329–334.
[27] E.M. Spiesz, P.K. Zysset, Structure–mechanics relationships in mineralized tendons, J. Mech. Behav. Biomed. Mater. 52 (2015) 72–84.
[28] H.S. Gupta, P. Messmer, P. Roschger, S. Bernstorff, K. Klaushofer, P. Fratzl, Synchrotron diffraction study of deformation mechanisms in mineralized tendon, Phys. Rev. Lett. 93 (15) (2004) 158101.
[29] C.A. Schneider, W.S. Rasband, K.W. Eliceiri, NIH Image to ImageJ: 25 years of image analysis, Nat. Methods 9 (7) (2012) 671–675.
[30] A.K. Maurya, L. Weidenbacher, F. Spano, G. Fortunato, R.M. Rossi, M. Frenz, A. Dommann, A. Neels, A. Sadeghpour, Structural insights into semicrystalline states of electrospun nanofibers: a multiscale analytical approach, Nanoscale 11 (15) (2019) 7176–7187.
[31] G. Siqueira, D. Kokkinis, R. Libanori, M.K. Hausmann, A.S. Gladman, A. Neels, P. Tingaut, T. Zimmermann, J.A. Lewis, A.R. Studart, Cellulose nanocrystal inks for 3D printing of textured cellular architectures, Adv. Funct. Mater. 27 (12) (2017) 10.
[32] R.C. Team, R: a Language and Environment for Statistical Computing, 2021. http://www.R-project.org/.
[33] H. Suhonen, M. Fernández, R. Serimaa, P. Suortti, Simulation of small-angle X-ray scattering from collagen fibrils and comparison with experimental patterns, Phys. Med. Biol. 50 (22) (2005) 5401–5416.
[34] B.A. Wright, Low-angle X-Ray diffraction pattern of collagen, Nature 162 (4105) (1948) 23-23.
[35] Y. Kudo, M. Sakuragi, S. Hashida, R. Kuwahara, T. Ishi-I, H. Masunaga, K. Sakurai, Flexibility and local structure of a worm-like cylinder of self-assembled discotic triazine triamide, Polym. J. 42 (10) (2010) 812–817.
[36] W. Ruland, Small-angle scattering studies on carbonized cellulose fibers, J. Polym. Sci. Part C Polym. Symp. 28 (1) (1969) 143–151.
[37] S. Ran, D. Fang, X. Zong, B.S. Hsiao, B. Chu, P.M. Cunniff, Structural changes during deformation of Kevlar fibers via on-line synchrotron SAXS/WAXD techniques, Polymer 42 (4) (2001) 1601–1612 (Guildf).
[38] T.A. Grünewald, M. Liebi, N.K. Wittig, A. Johannes, T. Sikjaer, L. Rejnmark, Z. Gao, M. Rosenthal, M. Guizar-Sicairos, H. Birkedal, M. Burghammer, Mapping the 3D orientation of nanocrystals and nanostructures in human bone: indications of novel structural features, Sci. Adv. 6 (24) (2020) eaba4171.
[39] W.J. Landis, M.J. Song, A. Leith, L. McEwen, B.F. McEwen, Mineral and organic matrix interaction in normally calcifying tendon visualized in three dimensions by high-voltage electron microscopic tomography and graphic image reconstruction, J. Struct. Biol. 110 (1) (1993) 39–54.